

# Parametric study of liquid metal flows in conducting circular ducts in a strong nonuniform magnetic field

S. Molokov<sup>a,b,\*</sup>, G. Politis<sup>a</sup>

<sup>a</sup> UK Atomic Energy Authority (UKAEA), Culham Science Centre, Abingdon, OX14 3DB, United Kingdom

<sup>b</sup> Technische Universität Ilmenau, Postfach 100565, 98684 Ilmenau, Germany

## ARTICLE INFO

### Keywords:

Liquid metal blankets  
Thermonuclear fusion  
Magnetohydrodynamics (MHD)  
Pressure drop

## ABSTRACT

Parametric study of main flow characteristics in magnetohydrodynamic flow in the exit duct from a liquid metal blanket has been performed. The flow in such a duct occurs in a nonuniform, decreasing magnetic field. The duct wall is electrically conducting. The wall conductance ratio,  $c$ , and the gradient of the field,  $\gamma$ , have been varied in a wide range,  $0.01 \leq c \leq 0.5$  and  $0.3 \leq \gamma \leq 0.8$  covering most of the cases relevant to fusion. The studies have been performed with asymptotic methods for high values of the Hartmann number and interaction parameter, as well as with FLUENT. Pressure drop correlation has been developed, which is important for blanket design. The results show a significant increase in three-dimensional effects with decreasing wall conductance ratio. For small values of  $c$ , a stagnant zone is present in the nonuniform field region for all the values of the field gradient, which may create difficulties for tritium removal. If the exit duct is very long, the three-dimensional pressure drop is relatively low, but the effect of the nonuniform magnetic field on the velocity profiles is significant.

## 1. Introduction

Magnetohydrodynamic (MHD) effects are important for all liquid metal blanket designs regardless of the liquid metal use as a breeder of tritium only or as a coolant as well. These effects strongly affect both the pressure drop, and heat- and mass- transfer due to high Lorentz forces resulting from the interaction of the induced electric currents with the magnetic field. These forces brake the flow, and restructure the velocity profiles. Owing to their importance, MHD effects in ducts have been studied for many decades. Comprehensive reviews on recent work in this area may be found in [1,2].

The blankets consist of many elements, such as expansions and contractions, manifolds and bends, etc. Each of these elements produces three-dimensional (3D) effects, which require proper modelling. Among the most important blanket elements are feeding and draining ducts supplying the liquid metal to the heating/breeding zones. Such ducts are almost always circular and may be either electrically conducting or nearly insulating depending on the blanket concept. As these ducts enter/leave the reactor area, the flow is subjected to a highly nonuniform magnetic field, and we will focus here on the flow in a circular conducting duct leaving the reactor area (Fig. 1).

In a high magnetic field, the flow region splits into the inviscid core and viscous Hartmann- and Roberts- layers at the duct wall (Fig. 2) [3–5]. This division exists even for a duct in a uniform field. In fusion

related applications, the thickness of these layers is just a few microns. This is where the core velocity falls to zero owing to the no-slip condition at the wall. The layers may become somewhat thicker if the flow becomes weakly turbulent, but a conducting wall tends to prevent it owing to high electromagnetic damping. There are small overshoots of velocity in the Roberts layers [6,7] (Fig. 3), but they do not affect the flow balance between the core and the layers, and can easily be neglected.

Consider now the nonuniform field region. If the wall is much better conductor than the Hartmann layer ( $c \gg Ha^{-1}$ ), and  $c^{1/2}$  is small ( $c^{1/2} \ll 1$ ), the fluid follows *characteristic surfaces* [8], a concept introduced earlier by Kulikovskii [9] for electrically insulating geometries. Here  $c$  is the wall conductance ratio, and  $Ha$  is the Hartmann number. Some of these surfaces, closer to the Roberts layers, provide a path for the fluid from upstream to downstream. But there are surfaces with an origin at the axis of the duct in the nonuniform field region that do not allow the fluid to pass freely. Then the fluid encompassed by them is blocked [8,9], and a (nearly) stagnant zone appears. As a result, the fluid is pushed towards the sides, flowing around a stagnant zone (Fig. 4), and an M-shaped velocity profile is formed in the nonuniform field region. The fluid requires very high distances to cross the characteristic surfaces and thus to restructure, so that the effect of the nonuniform field is ‘felt’ by the flow at distances extending to many

\* Corresponding author at: UK Atomic Energy Authority (UKAEA), Culham Science Centre, Abingdon, OX14 3DB, United Kingdom.  
E-mail address: [sergei.molokov@ukaea.uk](mailto:sergei.molokov@ukaea.uk) (S. Molokov).

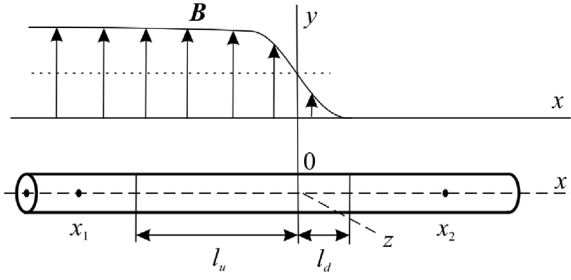


Fig. 1. Liquid metal flow in a circular exit pipe of radius  $R$  in a nonuniform, decreasing magnetic field. Pressure measurements are taken between points  $x = x_1$  and  $x = x_2$ . The development lengths upstream and downstream are  $l_u$  and  $l_d$ , respectively;  $(x, y, z)$  are Cartesian co-ordinates.

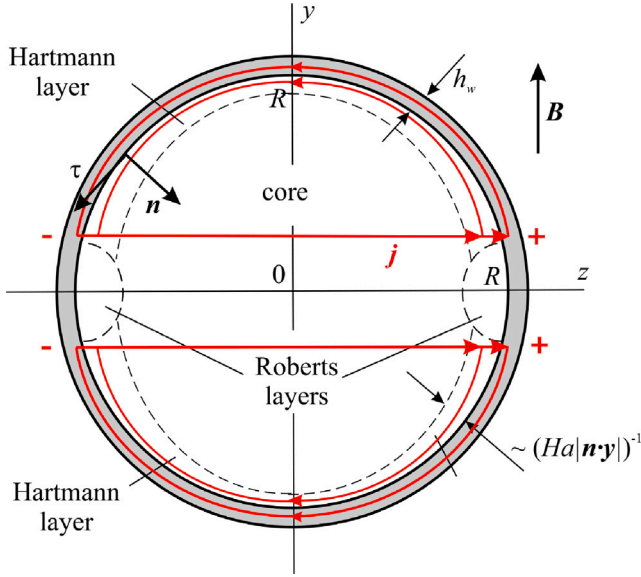


Fig. 2. Flow subregions for  $Ha \gg 1$ : inviscid core, and viscous Hartmann and Roberts layers. Induced currents are shown in red. The signs “+” and “-” indicate induced potential difference between the right and left parts of the duct.

duct radii. Such distances upstream and downstream are called the *development lengths*  $l_u$  and  $l_d$ , respectively.

Walker [10] improved and upgraded this solution, and removed discontinuities in the velocity profiles. It was shown that the structure of the flow in the nonuniform field region is more complicated than previously thought with additional boundary and internal layers present in the flow. However, in the experiments [11,12], the value of  $c^{1/2}$  was not sufficiently small. For example, for  $c = 0.027$  [12], one gets  $c^{1/2} = 0.52$ , and thus a different, improved theory was required, not bound by the constraint  $c^{1/2} \ll 1$ . Such a theory was developed in [13]. The agreement with Reed’s experiment was nearly perfect [12], and we will use this theory here. The main feature of this asymptotic solution for arbitrary value of  $c$  was that there was only a qualitative tendency of the flow to follow the characteristic surfaces, and the development lengths were not as high as was previously predicted. As the experimental data in [12] was available, it was designated as one of the benchmark problems for testing Computational Fluid Dynamics (CFD) codes [14]. Comparisons with Reed’s experiment were performed in a number of papers (see a review in [14] and Refs. [15,16]).

In most of the references with the exception of [17], the results were presented for just one set of governing parameters,  $c$ ,  $Ha$ , and

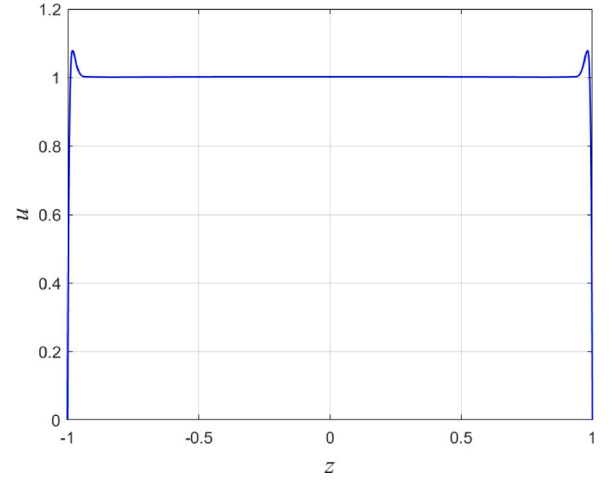


Fig. 3. Axial velocity profile in a fully developed flow in the symmetry plane  $y = 0$ , perpendicular to the uniform magnetic field, for the wall conductance ratio,  $c = 0.1$ , and for the Hartmann number,  $Ha = 2,681$ . Calculations have been performed by FLUENT.

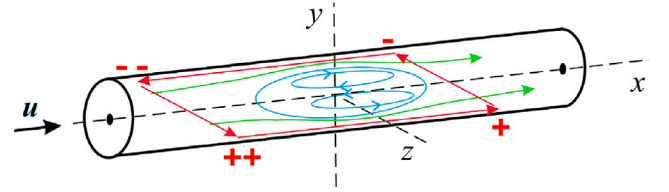


Fig. 4. Schematic diagram of the fluid flow around a stagnant zone in the nonuniform field region. The signs “++” and “--” indicate higher potential difference upstream than downstream.

$N$ , and for one value of the field gradient. Here  $N$  is the interaction parameter. For blanket design it is desirable to know main flow characteristics, such as the minimum and the maximum of velocities, the development lengths, etc., and to have pressure drop correlation for a wide range of parameters relevant to fusion. This is the main topic of this investigation.

## 2. Formulation

Consider an isothermal flow of viscous, incompressible, electrically conducting fluid along a straight circular duct of radius  $R$  in the  $x$ -direction in a strong, transverse magnetic field  $\mathbf{B} = B(x)e_y$  normalised by  $B_0$ , the maximum field inside the magnet. Function  $B(x)$  defines the dimensionless variation of the field along the flow, and  $(x, y, z)$  are Cartesian co-ordinates. The duct wall is thin and is electrically conducting.

The dimensionless equations governing the flow in the inductionless approximation are [18]:

$$Ha^{-2}\nabla^2\mathbf{u} + \mathbf{j} \times \mathbf{B} = \nabla p + N^{-1} \left\{ (\mathbf{u} \cdot \nabla)\mathbf{u} + \frac{\partial \mathbf{u}}{\partial t} \right\}, \quad (1)$$

$$\mathbf{j} = -\nabla\phi + \mathbf{u} \times \mathbf{B}, \quad (2)$$

$$\nabla \cdot \mathbf{u} = 0, \quad (3)$$

$$\nabla \cdot \mathbf{j} = 0. \quad (4)$$

The length, the time,  $t$ , the fluid velocity,  $\mathbf{u} = (u, v, w)$ , the electric current density,  $\mathbf{j}$ , the electric potential,  $\phi$ , and the pressure,  $p$ , are normalised by  $R$ ,  $R/u_0$ ,  $u_0$ ,  $\sigma u_0 B_0$ ,  $Ru_0 B_0$ , and  $R\sigma u_0 B_0^2$ , respectively, where  $u_0$  is the average fluid velocity, and  $\sigma$  is its electrical conductivity. The dimensionless parameters are the Hartmann number,

$Ha = RB_0(\sigma/\rho\nu)^{1/2}$ , and the interaction parameter,  $N = R\sigma B_0^2/\rho u_0$ . The Reynolds number,  $Re$ , can be expressed as follows:  $Re = Ru_0/\nu = Ha^2/N$ . Here  $\rho$  and  $\nu$  are the density and the kinematic viscosity of the fluid, respectively.

The boundary conditions are the no-slip condition for the fluid velocity, and the electrical condition for a thin-wall duct, namely

$$\mathbf{u} = 0 \quad \text{at the wall,} \quad (5)$$

$$\mathbf{j} \cdot \mathbf{n} = c\nabla_{\tau}^2 \phi \quad \text{at the wall,} \quad (6)$$

where  $c = \sigma_w h_w / \sigma R$  is the wall conductance ratio,  $\sigma_w$  and  $h_w$  are the electrical conductivity and the thickness of the wall, respectively,  $\mathbf{n}$  is the inward unit vector normal to the wall, and  $\nabla_{\tau}^2$  is the Laplace operator in the plane of the wall.

### 3. Asymptotic and numerical models

We employ two different models to solve Eqs. (1)–(6): the asymptotic model and the CFD one. They are described below.

#### 3.1. Asymptotic model (AM)

The asymptotic model (AM) takes advantage of the fact that the magnetic field in fusion is strong, which implies that  $Ha \gg 1$  and  $N \gg 1$ , so that inertia is neglected, while viscous forces act only in the boundary layers at the duct wall. Then the flow region splits into various subregions with different balance of forces (Fig. 2). In particular, in the inviscid, inertialess core, which occupies most of the duct cross-section, the pressure becomes two-dimensional, independent of the co-ordinate along the field provided the flow is isothermal. This allows integration of the equations in the field direction. The resulting equations in two dimensions transverse to the magnetic field are solved either analytically or numerically.

We assume that  $c \gg Ha^{-1}$ , i.e. that the wall is a much better conductor than the Hartmann layers. This implies that all the current induced in the core enters the wall and flows along it to other parts of the duct bypassing the layers (Fig. 2). Then the Hartmann number completely scales out of the problem, and the governing equations for the core pressure,  $p_c(x, \theta)$ , and the wall potential,  $\phi_w(x, \theta)$ , are [13]:

$$\begin{aligned} \frac{\partial}{\partial \theta} \left[ \left( \beta^2 + \frac{1}{3} \beta'^2 \cos^2 \theta \right) \frac{\partial p_c}{\partial \theta} \right] + \cos^2 \theta \frac{\partial}{\partial x} \left( \beta^2 \frac{\partial p_c}{\partial x} \right) \\ = \beta' \cos \theta \frac{\partial \phi_w}{\partial \theta} + \beta \sin \theta \frac{\partial \phi_w}{\partial x}, \end{aligned} \quad (7)$$

$$c \left[ \frac{\partial^2 \phi_w}{\partial \theta^2} + \frac{\partial \phi_w^2}{\partial x^2} \right] = \beta' \cos \theta \frac{\partial p_c}{\partial \theta} + \beta \sin \theta \frac{\partial p_c}{\partial x}, \quad (8)$$

where  $\theta = \arcsin z$ ,  $z = \sin \theta$ ,  $\beta = B^{-1}(x)$ , and  $\beta' = d\beta/dx$ .

The boundary conditions are:

$$\frac{\partial p_c}{\partial x} = -\frac{c}{1+c} B_u^2, \quad \frac{\partial \phi_w}{\partial x} = 0 \quad \text{at } x = x_1, \quad (9)$$

$$p_c = 0, \quad \frac{\partial \phi_w}{\partial x} = 0 \quad \text{at } x = x_2, \quad (10)$$

$$\frac{\partial p_c}{\partial \theta} = 0, \quad \phi_w = 0 \quad \text{at } \theta = 0, \quad (11)$$

$$\frac{\partial p_c}{\partial \theta} = 0, \quad \frac{\partial \phi_w}{\partial \theta} = 0 \quad \text{at } \theta = \frac{\pi}{2}. \quad (12)$$

Here points  $x_1$  and  $x_2$  define the computational domain in the  $x$ -direction. They can also be the measurement points for pressure. The pressure boundary condition in Eq. (9) follows from [4]. The solution for the Hartmann layers can easily be obtained analytically and added to the core. The problem for the 3D Roberts layers is complicated, but as they are passive, the solution for them is not necessary for the purpose of this study.

All the flow variables, such as velocities, currents, and core potential, can be expressed in terms of  $p_c(x, \theta)$  and  $\phi_w(x, \theta)$ . In particular, the axial component of velocity in the plane  $y = 0$  is

$$\begin{aligned} u_c = -\frac{1}{2} \beta \beta' \left\{ \frac{\partial^2 p_c}{\partial \theta^2} - \tan \theta \frac{\partial p_c}{\partial \theta} \right\} - \beta^2 \frac{\partial p_c}{\partial x} \\ + \beta \sec \theta \frac{\partial \phi_w}{\partial \theta} \quad \text{at } y = 0. \end{aligned} \quad (13)$$

Eqs. (7)–(12) have been solved numerically by finite differences on a collocated mesh. The  $x$ -co-ordinate has been transformed analytically into co-ordinate  $s$  with clustering of grid points in the nonuniform field region and continuously stretching them away from it in both directions. The resulting equations have been solved by central differences in the  $(s, \theta)$ -plane. The grid involves  $256 \times 32$  intervals. The difference equations have been solved using a direct linear equation solver for sparse matrices. The details of the scheme may be found in [19].

#### 3.2. CFD model (FLUENT)

The computational analysis was performed using ANSYS FLUENT 2023R2, which employs the finite-volume method to solve the governing equations. A pressure-based coupled solver was utilised, featuring second-order approximations for the pressure gradient and a second-order upwind scheme for the convective terms in the momentum equation. This upwind scheme requires cell-centred values and cell-centred gradients in the upstream cell. To compute these gradients, the Least Squares Cell-Based scheme was employed. The simulations used a pseudo-transient solution algorithm, assuming a laminar flow regime. The built-in inductionless Magnetohydrodynamics (MHD) solver enabled coupling of hydrodynamic equations with Maxwell's equations. The simulation geometry was meshed using ANSYS Meshing. In the radial direction, the first element size in the inflation layer of the fluid domain was set to  $10^{-6}$  meters, with an inflation growth rate of 1.15, ensuring approximately 10 cells within the Hartmann layer ( $R/Ha$ ). For the solid domain, the first element size was identical, with the growth rate adjusted to 1.4. This consistency in element size across the solid/fluid interface is crucial as varying element sizes can impede the stability and performance of the code, potentially affecting the results. The resulting mesh in the  $(y, z)$ -cross-section is shown in Fig. 5. In the axial direction, a discretisation bias of approximately 5 was applied from the inlet/outlet towards  $x = 0$  to elongate elements outside the nonuniform magnetic field region and to ensure sufficient element density near  $x = 0$ . This meshing strategy resulted in approximately 10 million elements, with an average orthogonal quality of 0.993 and a maximum skewness of 0.3407.

#### 3.3. Validation of the models

The models have been validated by comparing the results between themselves, as well as by comparing with the experiment in [12]. The results for the axial pressure gradient at  $y = 0$ ,  $z = 1$  shown in Fig. 6 are in very good agreement with the experiment.

## 4. Results

Here we present the results for the tanh-family of fields [12,19]:

$$B(x) = \frac{1}{2}(B_d + B_u) + \frac{1}{2}(B_d - B_u) \tanh(\gamma x), \quad (14)$$

where  $B_u$  and  $B_d$  are the values of the uniform magnetic field upstream and downstream, respectively, and

$$\gamma = |dB/dx|_{max} = |dB/dx|_{x=0} \quad (15)$$

is the maximum value of the dimensionless field gradient. Such fields are characteristic for two-pole magnets [12,20]. The field for the exit pipe ( $B_u = 1$ ,  $B_d = 0.01$ ) and for three typical values of  $\gamma$  is shown in Fig. 7. The value  $\gamma = 0.45$  corresponds to the field in ALEX facility at

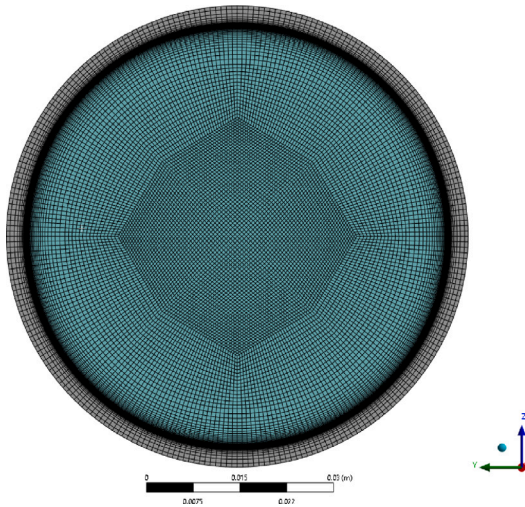


Fig. 5. Mesh in the  $(y, z)$ -cross-section used in calculations with FLUENT.

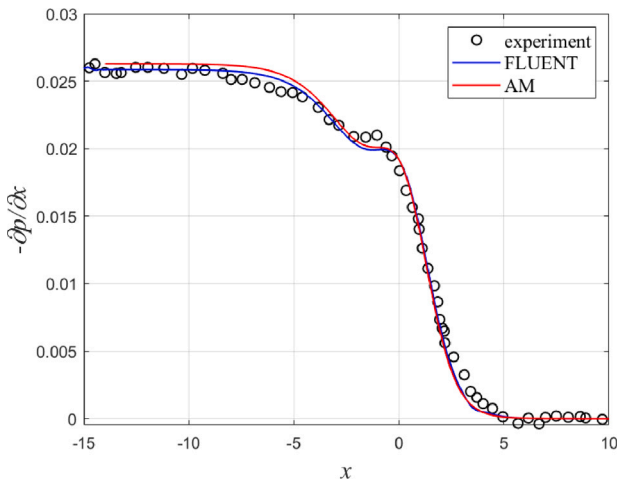


Fig. 6. Negative value of the axial pressure gradient at  $y = 0$ ,  $z = 1$  for  $c = 0.027$ ,  $\gamma = 0.45$ ,  $Ha = 6,600$  and  $N = 10,700$ . The field (14) in the experiment [12] was shifted along  $x$  by 0.4.

ANL. The value  $\gamma = 0.3$  gives a gradually varying field over 20 duct radii, while  $\gamma = 0.8$  gives a step-like field, which produces strongest 3D effects. The value of  $B_d$  is not exactly equal to zero but is set to a small value as it is important for the asymptotic equations not to become singular. This affects the results only by a very small amount. The origin of the co-ordinate system,  $x = 0$ , is at the point, where all the curves in Fig. 7 intersect, and this is where the field is equal to the average between the upstream and the downstream values. The dimensional field gradient linearly depends on the pipe radius as follows from scaling. Thus, for the same dimensional field gradient and different radii of the duct, one gets different values of  $\gamma$ .

#### 4.1. The results for PbLi and of Li

The results in this Section are presented for the following input data:

$$R = 3.4 \text{ cm}, u_0 = 1 \text{ mm/s}, B_0 = 4 \text{ T}, \gamma = 0.45, \\ h_w = 3 \text{ mm}, \sigma_w = 1,155,167 \text{ S/m}, \quad (16)$$

and for the values of material properties and dimensionless parameters given in Table 1. The wall is made of stainless steel. Most of these values are typical for future experiments in the CHIMERA facility at

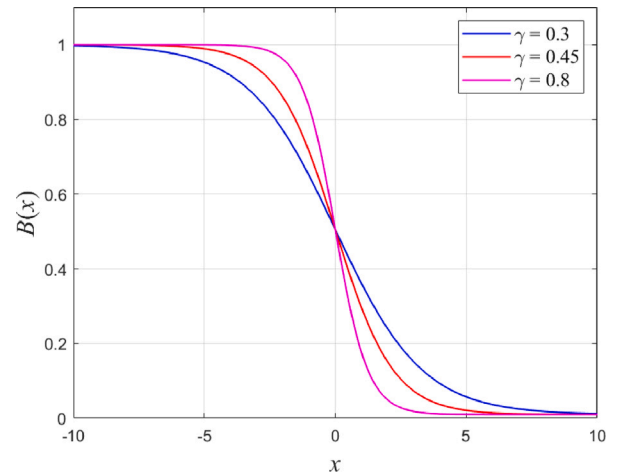


Fig. 7. The magnetic field for the exit pipe for three values of the maximum field gradient.

Table 1

Material properties and dimensionless parameters of PbLi and Li [22,23] at 320 °C.

Parameter	PbLi	Li
$\rho$ , kg/m <sup>3</sup>	9814	503
$\sigma$ , S/m	876,942	3,203,507
$\nu$ , m <sup>2</sup> /s	$2.019 \times 10^{-7}$	$8.641 \times 10^{-7}$
$Ha$	2,861	11,679
$N$	48,610	3,466,920
$Re$	168.4	39.3
$c$	0.1162	0.0318

UKAEA [21]. The value of typical average velocity is 10 times smaller to remain within the laminar flow regime. This is discussed in Section 5.

Physical effects in duct flows in a nonuniform magnetic field are known qualitatively since 1960s [18,24,25]. They are briefly outlined here for the sake of clarity.

When the magnetic field is uniform, the flow is fully developed. An electric current  $\mathbf{j}$  is induced by the electromotive force  $\mathbf{u} \times \mathbf{B}$ . The current flows strictly in the  $(y, z)$ -plane as shown schematically in Fig. 2. The current loops must be closed, so it enters either the Hartmann layer or the electrically conducting wall choosing a path of least resistance, and flows along them to the opposite side of the duct cross-section. Thus, what we have is an electric circuit with two parallel resistances:  $c^{-1}$  for the wall, and  $Ha$  for the Hartmann layer. As the wall here is assumed to be a much better conductor than the Hartmann layer, it is the wall that is mainly responsible for the flow dynamics.

When the magnetic field is nonuniform, an electric potential difference appears along the flow as shown in Fig. 4, which is caused by the decreasing values of  $\mathbf{u} \times \mathbf{B}$ . This results in 3D currents with non-zero  $x$ -component. These 3D currents form loops as shown in the figure, and provide an additional braking force on the flow, especially at the centre of the duct cross-section. The liquid metal finds a way around it and flows close to the periphery of the duct cross-section bypassing the centre. Fig. 8 shows the development of the axial component of core velocity in the plane  $y = 0$ . One can see that the core velocity does not change along the flow both far upstream and far downstream of the nonuniform field region. As the fluid approaches this region (actually, somewhat before that as we will see below), restructuring of the velocity profile occurs. Jets appear in the planes transverse to the magnetic field close to both  $z = -1$  and  $z = 1$  as the fluid tries to bypass the region of high braking. The jets are thick as they are part of the core. Numerical values of the maximum velocity for both PbLi and Li are shown in Table 2. The jets are higher for Li as  $c$  is lower. If the value of  $c$  was made to decrease further, the wall would

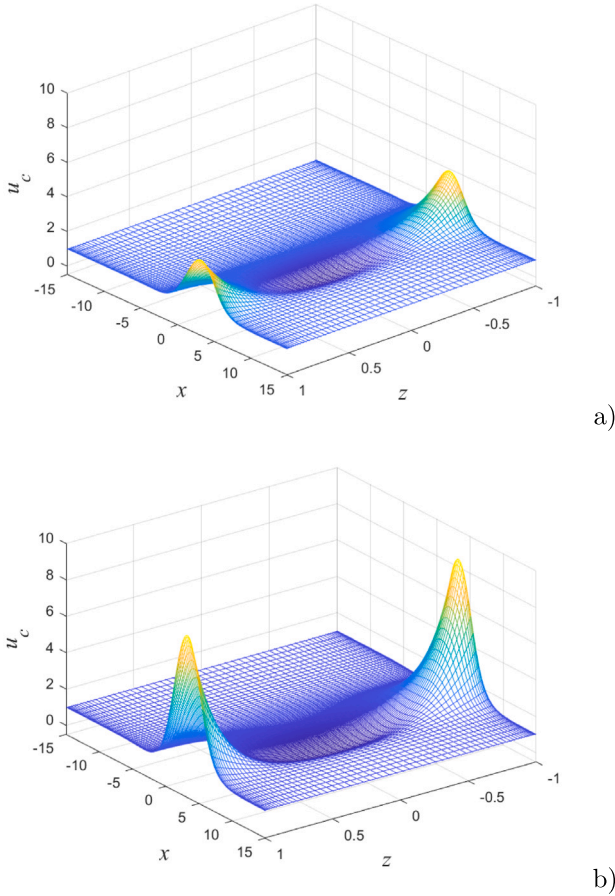


Fig. 8. Core velocity profiles in the mid-plane  $y = 0$  transverse to the magnetic field for PbLi (a) and for Li (b). (AM).

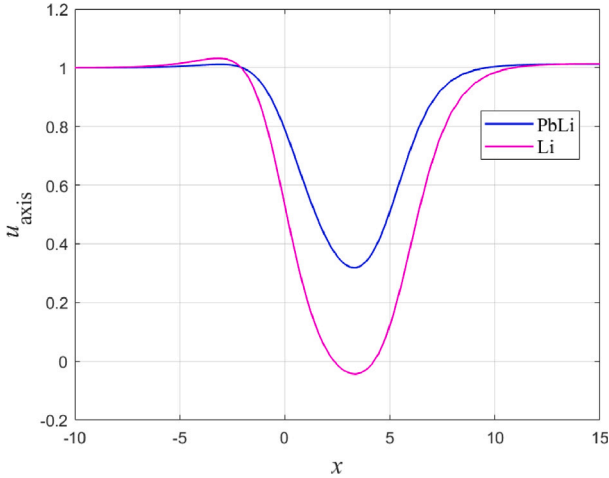


Fig. 9. Development of the core velocity along the duct axis. (AM).

start behaving qualitatively like an insulating one, and the velocity of the jets would be even higher (see [19] for comparison). Note that it is the maximum of core velocity that is shown in Table 2. For a finite Hartmann number, the maximum would be slightly different as viscous forces in the Roberts layers would act to smooth-out the maxima while reducing the velocity to zero at the wall (see below). It is interesting that the maxima (and the minima) of core velocity occur at  $x = 3.36$ , i.e. at the end of the nonuniform field region.

The minimum of the core velocity occurs at the duct axis (Fig. 9). There is no stagnant zone for PbLi as  $u_{min} > 0$ . However,  $u_{min}$  is negative for Li albeit being very small. This implies that there are two weakly recirculating vortices in the stagnant zone of length  $l_{st} = 2.779$  duct radii as shown schematically in Fig. 4. The importance of the presence of the stagnant zone and a weak recirculating flow there may become quite significant for the exit duct as outgoing tritium may accumulate there, and the only way to recover it would be through diffusion.

Consider now the pressure distribution. In the fully developed flow far upstream and far downstream, the pressure falls linearly with  $x$ , so that the pressure gradients are constant, equal to

$$(dp/dx)_u = -\frac{c}{1+c} B_u^2 \text{ for } x < -l_u,$$

$$(dp/dx)_d = -\frac{c}{1+c} B_d^2 \text{ for } x > l_d.$$

As the fluid approaches the region of the nonuniform field, transverse pressure difference appears due to 3D currents (Fig. 10). Besides, there is an additional, 3D pressure drop along the flow caused by these currents, which is denoted by  $\Delta p_{3D}$ . There are two most popular ways to define it. The first one is to extend the constant pressure gradients in fully developed flows far upstream and far downstream to the point  $x = 0$ , and then to calculate the difference in their values [8,11,19]. To define the second one, we need to introduce the notion of a locally fully developed flow. It is the flow in which the core velocity is equal to one for all values of  $x$ , while the pressure gradient is defined by a local value of the magnetic field. Such a flow is realistic but only for the magnetic field changing very gradually over very long distances, so that 3D effects become negligibly small in the whole flow domain. Thus, the second way to define  $\Delta p_{3D}$  is to calculate the difference between the total pressure drop  $\Delta p$  and the one in locally fully developed flow,  $\Delta p_{lfd}$  [26]. Here we use the second definition.

As the pressure gradient in the locally fully developed flow is:

$$\frac{dp_{lfd}}{dx} = -\frac{c}{1+c} B^2(x), \quad (17)$$

then

$$\Delta p_{lfd} = \frac{c}{1+c} \int_{x_1}^{x_2} B^2(\xi) d\xi. \quad (18)$$

Thus,

$$\Delta p_{3D} = \Delta p - \Delta p_{lfd}. \quad (19)$$

Correlations for  $\Delta p_{3D}$  will be derived further in the text. Eq. (18) is widely known as Miyazaki correlation for the pressure drop [27]. It completely ignores 3D effects.

The significance of the 3D pressure drop compared to that in a fully developed flow can be quantified by the so-called 3D length. This is an additional duct length by which the straight duct with a uniform field needs to be extended to account for  $\Delta p_{3D}$ :

$$d_{3D} = |\Delta p_{3D} / (dp_c/dx)_u|. \quad (20)$$

The quantities characterising the 3D effects are presented in Table 2. For the reference flows of both PbLi and Li, the 3D length does not exceed one duct radius. If the distance between measurement points is high, the contribution of the 3D pressure drop into the total one is negligible, and Miyazaki expression (18) would give the value of  $\Delta p$  with good accuracy, such as in [28].

The development length upstream,  $l_u$ , is defined as the distance from point  $x = 0$  upstream, when the relative, transverse pressure difference,

$$\left| \frac{p_c(x, 0) - p_c(x, \pi/2)}{p_c(x, \pi/2)} \right|$$

first becomes less than some small constant,  $\epsilon$ . In these calculations,  $\epsilon = 0.01$  is taken. The development length downstream,  $l_d$ , is defined in a similar way. For the exit pipe,  $l_d$  is not very important. From Table 2 follows that  $l_u \sim 6$ . This is not very high, which contrasts with the flow in the insulating pipe [19].

**Table 2**  
Summary of key characteristics of the flow for input data (16).

Quantity	Notation	PbLi	Li
maximum velocity	$u_{max}$	3.879	8.421
minimum velocity	$u_{min}$	0.318	-0.043
position of minimum and maximum	$x_{max}$	3.360	3.360
pressure drop in the fully developed flow per unit length	$(-dp_c/dx)_u$	0.104	0.031
3D pressure drop	$\Delta p_{3D}$	0.034	0.026
3D length	$d_{3D}$	0.330	0.851
development length upstream	$l_u$	5.483	6.790
development length downstream	$l_d$	9.114	11.249
length of the stagnant zone	$l_{st}$	0	2.779

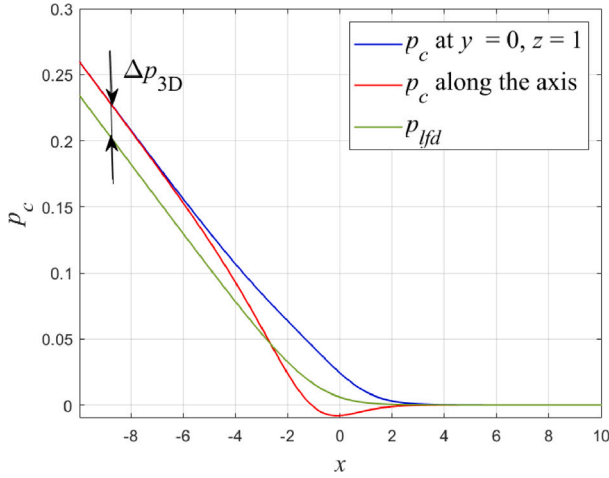


**Fig. 10.** Distribution of core pressure in Li flow along the duct axis and along  $z = 1$  at  $y = 0$ ; pressure in a locally fully developed flow, and the definition of the 3D pressure drop  $\Delta p_{3D}$ . (AM).

It also follows from Table 2 that the 3D effects in Li are much stronger than in PbLi (with the exception of  $\Delta p_{3D}$ ). For a fixed  $\gamma$  this is solely based on smaller value of parameter  $c$ . This observation will be discussed in the next Section.

#### 4.2. Variation of parameters and pressure drop correlation

Now we vary parameters  $c$  and  $\gamma$  in the fusion-relevant range,  $0.01 \leq c \leq 0.5$  and  $0.3 \leq \gamma \leq 0.8$ , and evaluate the most important quantities that characterise the flow. The effect of nonuniform magnetic fields on the velocity profiles may be very significant (Fig. 11a,b). This is especially so for low values of  $c$  and high values of  $\gamma$ . For  $c \sim 0.01$ , the maximum of core velocity exceeds 10 even for a gradually varying field.

For low  $c$ , a stagnant zone with recirculating flow exists for all values of  $c$ , and for all values of  $\gamma$  (Fig. 11b). For a step-like field, it persists up to  $c \sim 0.35$ , i.e. it is present even for a well-conducting wall for both PbLi and Li. This may be important as tritium may be trapped there. Typical axial velocity profiles in the nonuniform field region are shown in Fig. 12. The asymptotic solution for  $c = 0.001$  and  $Ha = 2,681$  is not shown in the figure as the condition of validity of the model,  $c \gg Ha^{-1}$  is violated. For higher values of  $c$ , the results obtained with AM and FLUENT are in very good agreement. The only difference is in the Roberts layers at  $z = \pm 1$ , which the current AM does not resolve. Calculations with FLUENT show that tiny overshoots of velocity exist only for sufficiently high conductivity of the wall, for  $c \geq 0.05$ . For lower values of  $c$ , they do not exist, and the role of the Roberts layers reduces to smoothing and matching the core velocity to zero at the wall owing to the no-slip condition.

For the range of parameters considered here, the effect of the nonuniform magnetic fields on the pressure drop is less significant than

on the velocity profiles. The log-log plots of the 3D pressure drop and the 3D length are shown in Figs. 11c and 11d, respectively. The 3D pressure drop first increases with increasing  $c$ , but then reaches a maximum within the range  $c \sim 0.2 - 0.4$  depending on the value of  $\gamma$ , and then it starts falling. This behaviour is typical for 3D MHD flows in conducting ducts (e.g. [29]). In the limit  $c \rightarrow \infty$ , i.e. when the wall becomes perfectly conducting,  $\Delta p_{3D} \rightarrow 0$  (not shown in the figure as it is outside of the fusion range). Indeed, for high  $c$ , the currents induced upstream along a highly conducting wall, do not need to flow downstream preferring to pass in the same duct cross-section. Conversely, if  $c$  decreases, the resistance of the circuit becomes high, the 3D currents become weak, and  $\Delta p_{3D}$  falls again. Weak currents imply that the term  $-\nabla\phi$  in Eq. (2) nearly fully compensates  $u \times B$  now. In a poorly conducting circuit potential differences rise, and so does the deformation of the velocity profile with them.

To obtain a correlation for the 3D pressure drop directly is not straightforward owing to its complex behaviour with varying  $c$  (Fig. 11c). But the 3D length falls nearly linearly with increasing  $c$  in the log-log plot (Fig. 11d) indicating a nearly power-law dependence of  $d_{3D}$  on  $c$ . To produce correlation for  $d_{3D}$ , several types of dependencies of this quantity on both  $c$  and  $\gamma$  have been tried, and the following one has been found to fit best:

$$d_{3D} \approx 0.173\gamma^{0.998}c^{(0.293\gamma-0.820)}. \quad (21)$$

Comparison between the data points (blue circles) and the fit (surface) in Fig. 13 shows that the agreement is very good. Thus,

$$\Delta p_{3D} = d_{3D} \left| \frac{dp_c}{dx} \right|_u \approx \frac{0.173}{1+c} \gamma^{0.998} c^{(0.293\gamma+0.180)}, \quad (22)$$

and the total, dimensional pressure drop is:

$$\Delta p^* = \sigma R u_0 B_0^2 [\Delta p_{lfd} + \Delta p_{3D}]. \quad (23)$$

Finally, the development length upstream reaches the value of 10 duct radii for  $c = 0.01$  and  $\gamma = 0.3$  (Fig. 14). For more steeply varying fields it is lower. It also decreases with increasing  $c$  underscoring the discussion above.

## 5. Discussion and conclusions

A parametric study of the flow in the exit pipe from the liquid metal blanket has been performed with the main aim to obtain the results for main flow characteristics for a conducting circular duct in a wide range of parameters relevant to fusion. Results of this work will enable to better predict phenomena in the future experiments in CHIMERA facility at UKAEA. The results show strong dependence of all the flow quantities on the wall conductance ratio,  $c$ , and the value of the axial gradient of the nonuniform magnetic field,  $\gamma$ . The Hartmann number and the interaction parameter play no role in the asymptotic model, which has been used to derive the pressure drop correlation. It is sufficient that both are high. The range of parameters covered involves perhaps most of the fusion and experimental range for a conducting pipe:  $0.01 \leq c \leq 0.5$  and  $0.3 \leq \gamma \leq 0.8$ .

As the value of  $c$  decreases, the three-dimensional (3D) effects become stronger. The effect on the velocity profiles is particularly high.

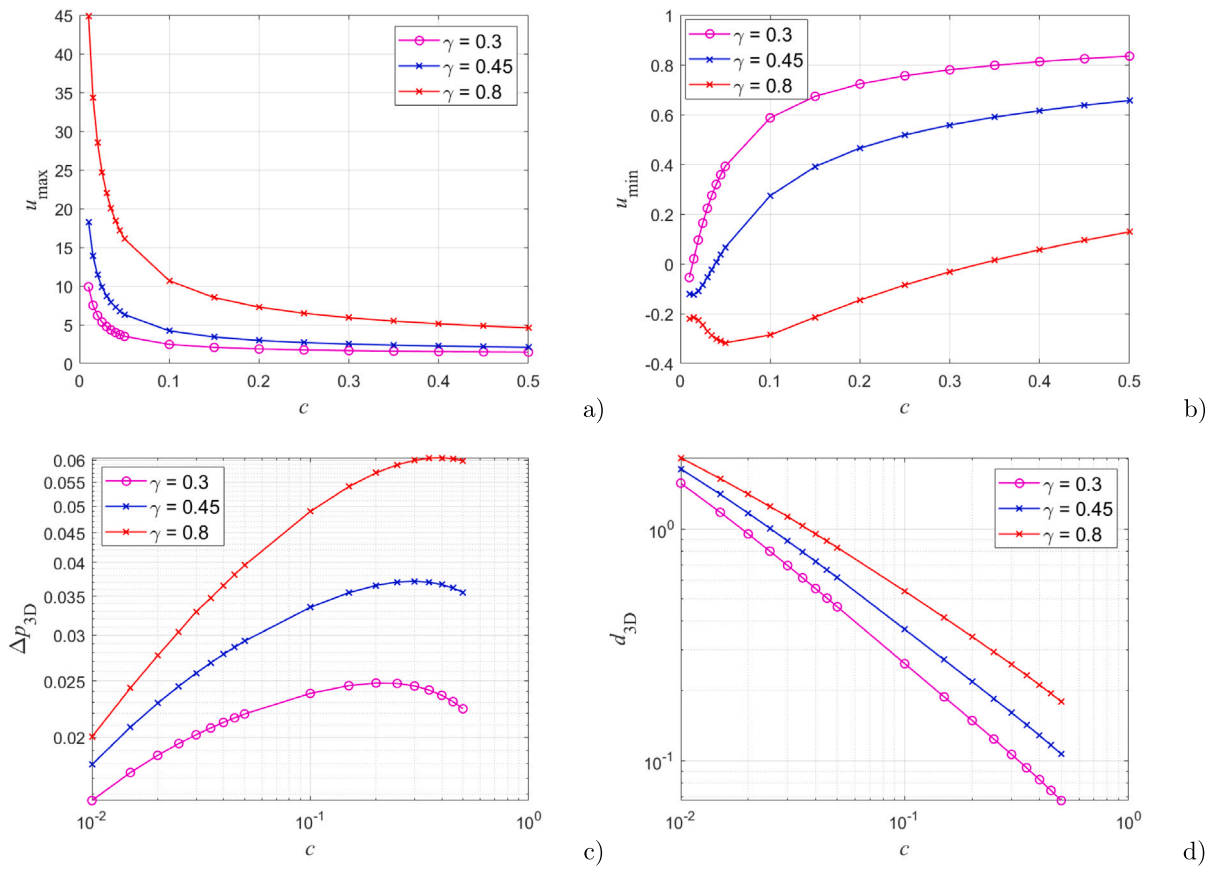


Fig. 11. Variation of maximum (a) and minimum (b) of core velocity at  $y = 0$ , and of the three-dimensional pressure drop (c) and the three-dimensional length (d) with  $c$  for three values of the field gradient. (AM).

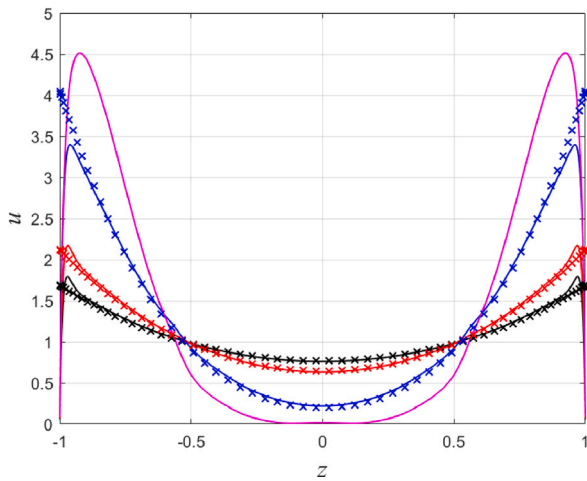


Fig. 12. Axial velocity profiles at  $y = 0$ ,  $x = 0$  for  $\gamma = 0.45$ ,  $Ha = 2,681$ , and  $N = 48,610$ . Solid lines correspond to calculations with FLUENT for  $c = 0.1$  (black), 0.05 (red), 0.01 (blue), and 0.001 (magenta). Corresponding AM values are shown with crosses of the same colour. The AM values for  $c = 0.001$  are not shown as the model becomes no longer valid for this value of  $Ha$ .

They become highly deformed involving thick jets as the fluid flows around the (nearly) stagnant zone at the centre of the nonuniform field region. The presence of the stagnant zone may adversely affect tritium recovery in the exit pipe.

The only quantity decaying with decreasing  $c$  is the 3D pressure drop. However, its contribution to the total pressure drop grows as

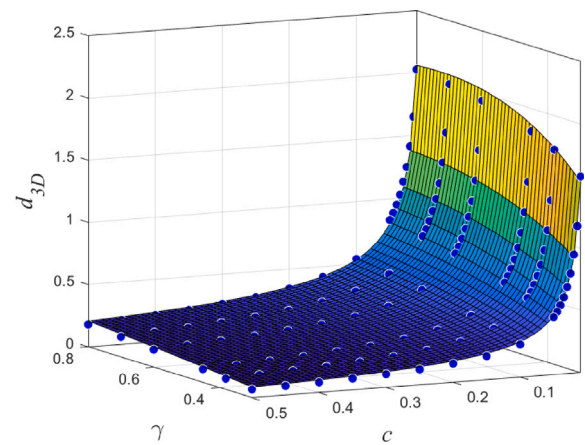


Fig. 13. Comparison between calculated values of the 3D length (blue circles) and the fit (21) (surface). (AM).

evidenced by the growth of the 3D length of the pipe. Despite this increase in the 3D length, it does not exceed one duct diameter even for a steep field at small values of  $c$ . This raises an important question regarding the significance of the 3D pressure drop in the overall estimation of the total pressure drop. If the distance between the measurement/reference points,  $x_1$  and  $x_2$  is high, for example covering the whole, long magnet, then it can easily be neglected and Miyazaki correlation can be used with success. But if  $x_2 - x_1$  is low, or if detailed measurements or modelling is required, then it becomes important. The best flow characteristic that determines this is the development length

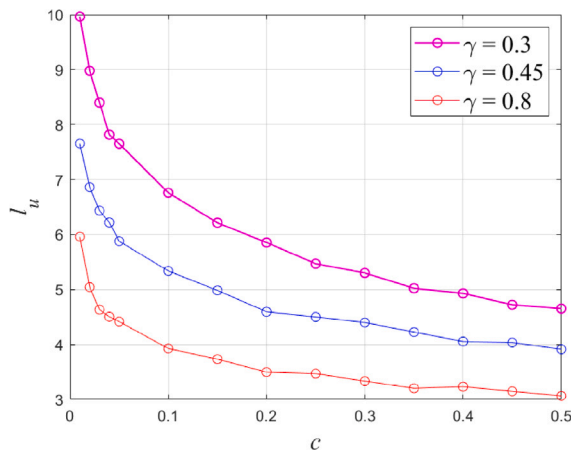


Fig. 14. Variation of the development length upstream with  $c$  for three values of the field gradient. (AM).

upstream, inside the magnet. Consider, for example, Fig. 5 in [13], where  $c = 0.02$ ,  $B_d = 0.5$ ,  $x_1 = -3$ ,  $x_2 = 6$ . Pressure was set to constants at both ends of the computational domain. It can be seen that the transverse difference in pressure appears right from the entrance to the domain, which implies that the 3D currents are blocked. Thus, the domain upstream is too short to account for all the 3D currents. Despite this shortfall, the model predicts that the total pressure drop deviates from the Miyazaki's expression by 10% over the length of 9 duct radii. Therefore, wherever the measurement points are, the computational domain upstream should be higher than the development length to produce a consistent, physically realistic model. This concerns any model whether an asymptotic- or a CFD- one.

Now, the pressure drop correlation presented here has been for the tanh-family of the magnetic fields. However, alternative magnetic configurations, such as those in the MEKKA facility at the Karlsruhe Institute of Technology [28], or within reactor environment, may result in different magnetic field variations along the duct, leading to distinct pressure drop correlations. Nonetheless, by adjusting the field gradient within the tanh-family, this correlation can serve as a preliminary approximation for pressure drop in these different configurations.

Finally, the correlation here has been produced using the inertialess asymptotic model as it is fast, so that many runs of the code could be performed within a reasonable time-frame. It works well for sufficiently high values of the interaction parameter, such as the one in [12]. For lower values, still relevant to fusion, inertial effects become important, see [28,30,31]. These effects are not straightforward, especially for the entrance pipe, and require a separate, thorough investigation.

#### CRedit authorship contribution statement

**S. Molokov:** Writing – review & editing, Writing – original draft, Validation, Methodology. **G. Politis:** Writing – review & editing, Writing – original draft, Validation, Software, Methodology.

#### Declaration of competing interest

The are no financial or other interests in submitting this work.

#### Acknowledgements

This work has been funded by the UK Government Department for Business, Energy & Industrial Strategy. No part of this paper may be reproduced without permission. To obtain further information on the data and models underlying this work please contact [PublicationsManager@ukaea.uk](mailto:PublicationsManager@ukaea.uk).

#### Data availability

To obtain further information on the data and models underlying this work please contact [PublicationsManager@ukaea.uk](mailto:PublicationsManager@ukaea.uk).

#### References

- [1] S. Smolentsev, Physical background, computations and practical issues of the magnetohydrodynamic pressure drop in a fusion liquid metal blanket, *Fluids* 6 (2021) 110, <http://dx.doi.org/10.3390/fluids6030110>.
- [2] C. Mistrangelo, L. Bühler, C. Alberghi, S. Bassini, L. Candido, C. Courtessole, A. Tassone, F.R. Ugorri, O. Zikanov, MHD R & D activities for liquid metal blankets, *Energies* 14 (2021) 6640, <http://dx.doi.org/10.3390/en14206640>.
- [3] J.A. Shercliff, The flow of conducting fluids in circular pipes under transverse magnetic fields, *J. Fluid Mech.* 1 (1956) 644, <http://dx.doi.org/10.1017/S0022112056000421>.
- [4] C.C. Chang, T.S. Lundgren, Duct flow in magnetohydrodynamics, *J. Appl. Math. Phys.* (ZAMP) 12 (1961) 100, <http://dx.doi.org/10.1007/BF01601011>.
- [5] P.H. Roberts, Singularities of Hartmann layers, *Proc. R. Soc. Lond. A.* 300 (1967) 94, <http://dx.doi.org/10.1098/rspa.1967.0159>.
- [6] S. Samad, The flow of conducting fluids through circular pipes having finite conductivity and finite thickness under uniform transverse magnetic fields, *Internat. J. Engrg. Sci.* 19 (1981) 1221.
- [7] S. Vantighem, X. Albet-Chico, B. Knaepen, The velocity profile of laminar MHD flows in circular conducting pipes, *Theor. Comput. Fluid Dyn.* 23 (2009) 525, <http://dx.doi.org/10.1007/s00162-009-0163-0>.
- [8] R.J. Holroyd, J.S. Walker, A theoretical study of the effects of wall conductivity, non-uniform magnetic fields and variable-area ducts on liquid-metal flows at high Hartmann number, *J. Fluid Mech.* 84 (1978) 471, <http://dx.doi.org/10.1017/S0022112078000282>.
- [9] A.G. Kulikovskii, Flows of a conducting incompressible liquid in an arbitrary region with a strong magnetic field, *Fluid Dyn.* 8 (1973) 462, <http://dx.doi.org/10.1007/BF01019975>.
- [10] J.S. Walker, Liquid-metal flow in a thin conducting pipe near the end of a region of uniform magnetic field, *J. Fluid Mech.* 167 (1986) 199, <http://dx.doi.org/10.1017/S0022112086002793>.
- [11] R.J. Holroyd, An experimental study of the effects of wall conductivity, non-uniform magnetic fields and variable area ducts on liquid metal flows at high Hartmann number. Part 2. Ducts with conducting walls, *J. Fluid Mech.* 96 (1980) 355, <http://dx.doi.org/10.1017/S0022112080002169>.
- [12] C.B. Reed, B.F. Picologlou, T.Q. Hua, J.S. Walker, ALEX results – a comparison of measurements from a round and a rectangular duct with 3-D code predictions, in: *12th Symposium on Fusion Engineering*, Monterey, California, October 13–16, IEEE, 1987, p. 1267.
- [13] G. Talmage, J.S. Walker, Three-dimensional laminar MHD flow in ducts with thin walls and strong magnetic fields, in: *Proc. 6th Beer-Sheva Seminar*, 1987, p. 3.
- [14] S. Smolentsev, S. Badia, R. Bhattacharyay, L. Bühler, L. Chen, Q. Huang, H.-G. Jin, D. Krasnov, D.-W. Lee, E. Mas de les Valls, C. Mistrangelo, R. Munipalli, M.-J. Ni, D. Pashkevich, A. Patel, G. Pulugundla, P. Satyamurthy, A. Snegirev, V. Sviridov, P. Swain, T. Zhou, O. Zikanov, An approach to verification and validation of MHD codes for fusion applications, *Fusion Eng. Des.* 100 (2015) 65, <http://dx.doi.org/10.1016/j.fusengdes.2014.04.049>.
- [15] J.-C. Feng, H.-L. Chen, Q.-Y. He, M.-Y. Ye, Further validation of liquid metal MHD code for unstructured grid based on OpenFOAM, *Fusion Eng. Des.* 100 (2015) 260, <http://dx.doi.org/10.1016/j.fusengdes.2015.06.059>.
- [16] D. Suarez, A. Khodak, E.M. de les Valls, L. Batet, A formal verification and validation of a low magnetic Reynolds number MHD code for fusion applications, *IEEE Trans. Plasma Sci.* 50 (2022) 4206, <http://dx.doi.org/10.1109/TPS.2022.3203801>.
- [17] G. Pulugundla, S. Smolentsev, T. Rhodes, C. Kawczynski, M. Abdou, Transition to a quasi-fully developed MHD flow in an electrically conducting pipe under a transverse non-uniform magnetic field, *Fusion Sci. Technol.* 68 (2015) 684, <http://dx.doi.org/10.13182/FST14-983>.
- [18] U. Müller, L. Bühler, *Magnetofluidynamics in Channels and Containers*, Springer, Dordrecht, 2001.
- [19] S. Molokov, C.B. Reed, Parametric study of the liquid metal flow in a straight insulated circular duct in a strong nonuniform magnetic field, *Fusion Sci. Technol.* 43 (2003) 200, <http://dx.doi.org/10.13182/FST03-A261>.
- [20] R.J. Holroyd, An experimental study of the effects of wall conductivity, non-uniform magnetic fields and variable-area ducts on liquid metal flows at high Hartmann number. Part 1. Ducts with non-conducting walls, *J. Fluid Mech.* 93 (1979) 609, <http://dx.doi.org/10.1017/S0022112079001956>.
- [21] T.R. Barrett, M. Bamford, N. Bowden, B. Chuilon, T. Deighan, P. Efthymiou, M. Gorley, T. Grant, D. Horsley, M. Kovari, M. Tindall, CHIMERA fusion technology facility: Testing and virtual qualification, *Fusion Sci. Technol.* 79 (2023) 1039, <http://dx.doi.org/10.1080/15361055.2022.2147766>.

- [22] D. Martelli, A. Venturini, M. Utili, Literature review of lead-lithium thermophysical properties, *Fusion Eng. Des.* 138 (2019) 183, <http://dx.doi.org/10.1016/j.fusengdes.2018.11.028>.
- [23] Thermophysical Properties of Materials for Nuclear Engineering: A Tutorial and Collection of Data, IAEA, Vienna, 2008, [https://www-pub.iaea.org/MTCD/Publications/PDF/IAEA-THPH\\_web.pdf](https://www-pub.iaea.org/MTCD/Publications/PDF/IAEA-THPH_web.pdf).
- [24] J.A. Shercliff, *The Theory of Electromagnetic Flow-Measurement*, Cambridge University Press, 1962, p. 146.
- [25] H. Branover, *Magnetohydrodynamic Flow in Ducts*, Wiley and Israel Universities Press, 1978, p. 290.
- [26] T.Q. Hua, J.S. Walker, B.F. Picologlou, C.B. Reed, Three-dimensional magnetohydrodynamic flows in rectangular ducts of liquid-metal-cooled blankets, *Fusion Technol.* 14 (1988) 1389.
- [27] K. Miyazaki, K. Konishi, S. Inoue, MHD pressure drop of liquid metal flow in circular duct under variable transverse magnetic field, *J. Nucl. Sci. Technol.* 28 (1991) 159, <http://dx.doi.org/10.1080/18811248.1991.9731336>.
- [28] V. Klüber, L. Bühler, C. Mistrangelo, Numerical simulation of 3D magnetohydrodynamic liquid metal flow in a spatially varying solenoidal magnetic field, *Fusion Eng. Des.* 156 (2020) 111659, <http://dx.doi.org/10.1016/j.fusengdes.2020.111659>.
- [29] S. Molokov, L. Bühler, Liquid metal flow in a U-bend in a strong uniform magnetic field, *J. Fluid Mech.* 267 (1994) 325, <http://dx.doi.org/10.1017/S0022112094001205>.
- [30] S. Molokov, C.B. Reed, Liquid metal MHD flows in circular ducts at intermediate Hartmann numbers and interaction parameters, *Magnetohydrodynamics* 39 (2003) 539.
- [31] X. Albets-Chico, D.G.E. Grigoriadis, E.V. Votyakov, S. Kassinos, Direct numerical simulation of turbulent liquid metal flow entering a magnetic field, *Fusion Eng. Des.* 88 (2013) 3108, <http://dx.doi.org/10.1016/j.fusengdes.2013.09.002>.